

# Resolving metal binding properties within subunits of a multimeric enzyme Mnx by surface induced dissociation and native ion mobility mass spectrometry

Deseree J Reid,<sup>1,§</sup> Stephanie M Thibert,<sup>2,§</sup> Jesse W Wilson,<sup>2,§</sup> Alexandra V Soldatova,<sup>3</sup> Bradley M Tebo,<sup>3,4</sup> Thomas G Spiro,<sup>3</sup> Mowei Zhou<sup>2,\*</sup> †

1. Chemical and Biological Signature Sciences, Pacific Northwest National Laboratory, 3335 Innovation Boulevard, Richland, WA, United States

2. Environmental Molecular Sciences Laboratory, Pacific Northwest National Laboratory, 3335 Innovation Blvd, Richland, WA 99354, United States

3. Department of Chemistry, University of Washington, Box 351700, Seattle, Washington 98195, United States

4. Division of Environmental and Biomolecular Systems, Institute of Environmental Health, Oregon Health & Science University, Portland, Oregon 97239, United States

\* corresponding: [moweizhou@zju.edu.cn](mailto:moweizhou@zju.edu.cn)

Present address:

† Department of Chemistry, Zhejiang University, Hangzhou, Zhejiang, China

§ These authors contributed equally.

## Keywords

Surface induced dissociation, metalloenzyme, native mass spectrometry, ion mobility, metal binding

## Abstract

Multi-subunit enzymes function as coordinated assemblies. Yet most enzymatic assays measure the summed output of all populations in solution and cannot easily differentiate contributions of individual subunits. Native mass spectrometry detects intact protein complexes in the gas phase. Surface induced dissociation further releases subunits from protein complexes while retaining compact conformations and bound ligands. Combined with ion mobility, the released subunits can then be carefully monitored for more in-depth structural analysis. Mnx is a unique bacterial multicopper oxidase complex that oxidizes Mn(II) to form MnO<sub>2</sub> minerals, and is composed of three subunits: MnxG, a multicopper oxidase containing the active site, and two accessory proteins, MnxE and MnxF which also bind copper ions. Other known multicopper oxidases do not require accessory proteins, therefore the functions of MnxE and MnxF are not well understood. Here, we use native mass spectrometry with surface induced dissociation and ion mobility to characterize the metal binding properties of Mnx with two metals, catalytic Cu(II) and Mn(II) substrate. We demonstrate our assay can detect subtle structural changes within each subunit, which are presumably related to the allosteric mechanism. We also noticed that ionic strength and solution composition can impact metal binding and must be carefully investigated for such experiments.

## Introduction

Multisubunit enzyme complexes possess expanded functional diversity via assembly and compartmentation of multiple enzymes, each serving unique structural, regulatory, or functional roles.[1-3] Structural and functional characterization of such enzymes can be challenging because of increased heterogeneity and reduced symmetry. Most experimental enzymatic assays measure the outcome of the full solution ensemble and do not easily differentiate functional contributions of each subunit in an enzyme complex.[2] Although structural biology methods can resolve more details, most experiments are resource- and labor-intensive. In addition, dynamic interactions and enzymatic reactions are challenging to capture and are often studied in discrete “snapshot” states.[4]

Native mass spectrometry (native MS) is capable of fast structural analysis of protein complexes, including dynamic systems.[5, 6] Ligand binding stoichiometry and affinity can be readily determined from native MS data. When coupled to ion mobility, conformational changes can also be probed. The sample consumption of native MS is often in the  $\mu\text{g}$  range, which is significantly lower than many commonly used methods, and enables screening of a broader range of conditions with limited input materials. A unique opportunity in native MS is to use various ion activation methods in the gas phase to dissect protein complexes and further characterize constituents in isolated states. This is particularly beneficial for studying multisubunit enzymes and elucidating the role of individual subunits. Collision-, electron-, and photon-based methods have all been applied to study protein complexes, providing complementary structural information.[7]

Herein, we present the characterization of metal-binding properties of a bacterial enzyme complex Mnx by native MS techniques. Mnx is a manganese-biomineralizing multicopper oxidase complex containing three proteins, MnxE, MnxF, and MnxG, at 3:3:1 stoichiometry. The assembly of Mnx— a hexamer ring of alternating MnxE and MnxF subunits attached to MnxG— was suggested by earlier native MS data.[8] It was confirmed by the recently solved structure of Mnx using cryo-electron microscopy assisted by AlphaFold prediction.[9] Mnx oxidizes Mn(II) and Mn(III), with the help of four catalytic Cu on the MnxG subunit, to form  $\text{MnO}_2$  minerals.[10, 11] The active site of MnxG is a well conserved structure among homologous multicopper oxidases, like human ceruloplasmin. MnxE and MnxF, which are essential for successful expression of the Mnx enzyme, have unknown function, but likely promote the release of  $\text{MnO}_2$  mineral products.[9] Previously, we used collision induced dissociation (CID) and surface induced dissociation (SID) to release subunits from Mnx in native MS, revealing that both MnxE and MnxF bind to Cu ions. SID was more effective than CID in releasing a near complete series of substructures for in-depth structural characterization, while better maintaining bound metal ions.[8, 12] In this study, we evaluate the interaction of Mnx with its substrate Mn(II). SID allowed us to monitor changes within each subunit. Although we did not detect the Mn binding state of Mnx in native MS likely due to short lifetime of the reaction intermediate, we observed reduced copper binding in MnxF, while MnxE retained its bound Cu after reacting with Mn. Limited  $m/z$  resolution prevented the identification of individually bound metal ions to the larger MnxG subunit, but its mass decreased slightly with increasing Mn. Drift times for all subunits increased after Mn was added, suggesting conformational changes after substrate turnover. We

also investigated the effects of adding Cu instead of Mn and found that the average number of bound Cu ions to MnxE and MnxF increased with increasing Cu concentration, and the mass of MnxG also increased. Unlike Mn addition, however, minimal changes in MnxE and MnxF drift times were observed in the presence of added Cu. Finally, we investigated metal binding of an inactive Mnx mutant where, unlike in the wild-type Mnx, Mn binding was observed due to a much slower turnover rate. Our results are consistent with the proposed allosteric mechanism of Mnx,[10] and demonstrate the unique potential of MS approach in comprehensive characterization of multisubunit enzymes.

### Material and methods

Mnx expression and purification, using the mnxEFG expression construct from *Bacillus* sp. PL-12, has been described previously.[13, 14] Metal acetates were purchased from Sigma and dissolved at desired concentration in deionized water. Mnx protein solution was buffer exchanged into 100 mM ammonium acetate at pH 7.8 using 7K Zeba microspin desalting columns (ThermoScientific, San Jose, United States), and diluted to ~ 3  $\mu$ M for native MS analysis. The MS data were acquired on a modified Synapt G2-Si ion mobility mass spectrometer (Waters Corporation, Manchester, United Kingdom) with a simplified SID design described previously.[15] Mass spectra were acquired between 500 and 12000  $m/z$  using 50 V sampling cone, 30 °C source temperature, 250 °C desolvation temperature, trap gas set to 5 mL/min, and the quadrupole set to manual mode at 6000  $m/z$  (biased transmission of higher mass species containing Mnx complexes). Data were acquired in ion mobility mode, with IMS wave velocity set to 450 m/s and IMS wave height set to 23 V. During SID experiments, the trap CE was set to 110 V, and collector and stopper voltages set to 100 V and 55 V, respectively. Samples were tested with 0–1000  $\mu$ M of the specified metal acetate with either no incubation—i.e., analysis was performed immediately after mixing—or after incubation at 4 °C overnight. Spectra were summed over 2–10 minutes, smoothed using +/- 20 windows and 10 smooths within the Waters MassLynx software. Each technical replicate was from either an individual MS experiment, or a subset of a long data acquisition. For a given experiment, each replicate has a similar number of spectral averages as specified in the metadata accompanying the raw data.

A specific region in the Driftscope containing mostly MnxG in SID was defined in the “rule” file, which was used to extract the MnxG peaks from the raw MS files. Each condition had triplicate datasets, either as separate MS experiments with different nanoESI capillaries, or as different segments of a long acquisition. MetaUniDec was used for mass spectral deconvolution.[16] We calculated the weighted average to estimate the average number of Cu bound to each subunit. Weighted averages for each replicate were calculated from peak areas normalized with respect to the total peak area, multiplied by their preassigned weights, summed, and then divided by 100. Weights were assigned as the number of bound Cu, i.e, 1Cu peaks were assigned a weight of 1, 2Cu peaks a weight of 2, etc.

The drift time profiles were extracted using TWIMExtract[17] and statistical analyses were performed on the extracted drift time profiles for each peak of interest (apo, +1 Cu, or +2 Cu) at each charge state. Briefly, drift time profiles were each fitted to a Gaussian and the peak maxima were compiled for each replicate. Next, a Shapiro-Wilk test was performed to check for

the normality of the data. Because all data were normal, a Bartlett test was used to verify homogeneity of variances. Finally, the difference in means was tested followed by Tukey's honest significant difference post-hoc test. Detailed information about source data files is included with raw data uploaded to MassIVE repository with accession MSV000092552.

## Results and Discussion

### *In vacuo dissection of Mnx complex differentiates metal binding to individual subunits*

Analysis of metal binding to individual MnxE/F/G monomers was achieved by mass isolation followed by dissociation of the Mnx complex by activation in the gas phase (Figure 1). The quadrupole was set to manual profile (set value at 6000  $m/z$ ), serving as high-pass filter for species larger than  $\sim 4200$   $m/z$ . The use of collision induced dissociation (CID) for subunit release was found previously to disrupt the weakly bound Cu on MnxF, and did not produce well resolved MnxG subunit.[8, 12] In contrast, surface induced dissociation (SID) results in a mixture of MnxE/F multimers, and MnxE/F/G monomers, with Cu-bound MnxE and MnxF maintained during subunit dissociation, suggesting that SID can maintain MnxE/F/G subunits in their folded states. Thus, when coupled with ion-mobility mass spectrometry, SID may be used to probe both the metal-binding stoichiometry of the individual monomer species, and changes in their structure upon metal binding by analyzing changes in drift time. The motivation of this work was to evaluate the changes in mass and drift time of MnxE/F/G monomers with increased Cu(II) and Mn(II) concentrations to better understand how Mnx behaves in response to the two metal ions. Mn(II) is the native substrate of Mnx, which Mnx efficiently turns over to form MnO<sub>2</sub>. Cu(II) is a native cofactor of Mnx that needs to be supplemented during protein expression to obtain an active enzyme. Understanding the interaction of these two metal ions with different Mnx subunits can provide clues to the unknown function of MnxE and MnxF.

To probe binding of Mn(II) to Mnx, we prepared Mnx wild-type (WT) samples with 0 – 1 mM Mn acetate in 100 mM ammonium acetate (AA) and directly infused samples onto the MS in ion mobility mode. Mnx complexes were then dissociated using SID and binding of Mn to the individual monomeric species was evaluated. Mn binding was not observed to any appreciable extent on any of the Mnx subunits (Figure 2A-B), presumably due to the fast catalytic rate of Mn oxidation by wild type Mnx (expected to complete the reaction in about 2 min or less). [10] Therefore, we examined the most abundant detectable species of MnxE and MnxF, to look at the effect of added Mn(II) substrate on the Cu metal centers there.

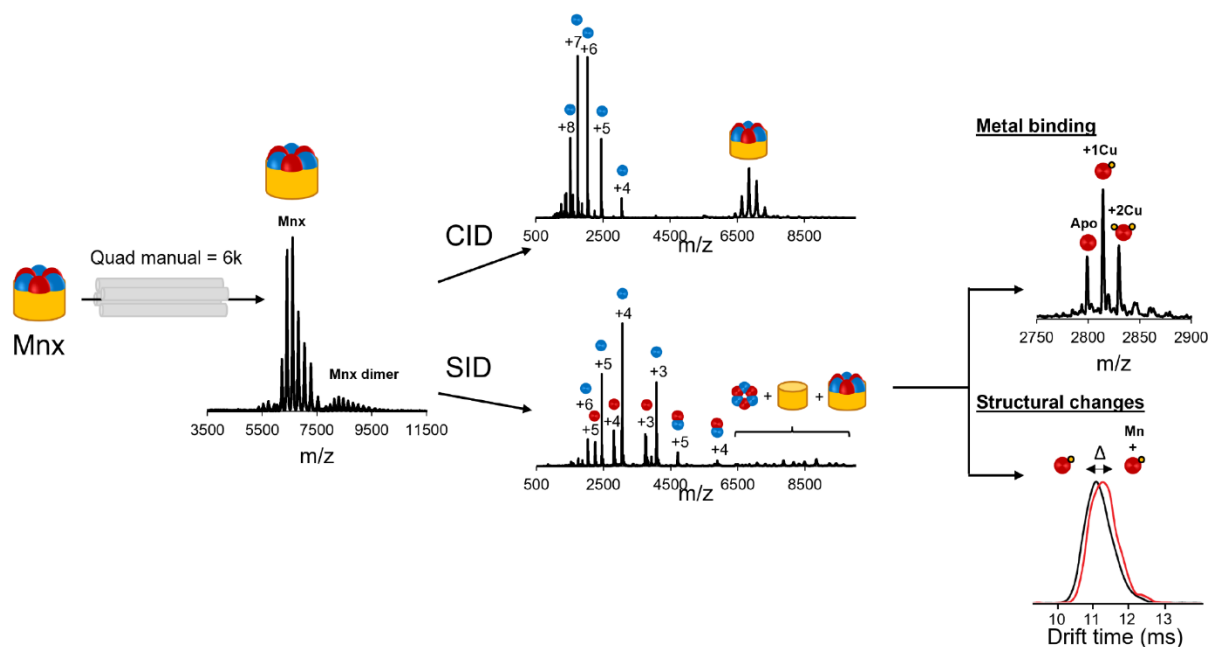


**Figure 1.** Workflow for metal-binding studies of MnxE/F/G monomers using ion mobility and surface induced dissociation (SID). While collision induced dissociation (CID) yields spectra primarily comprised of single monomer ejection, spectra obtained after SID result in a mixture of monomeric and multimeric species. Lower charge states of the ejected monomers after SID suggest this method better maintains folded structure of the monomer species and thus offers a method to monitor metal binding and structural changes upon changes in solution conditions, such as metal titrations.

Although binding of Mn was not observed on either MnxE or MnxF, decrease of Cu bound to MnxF occurred with increased Mn concentrations (Figure 2C). Copper ion ejection was not observed for the MnxE subunit, which maintained approximately 1 Cu bound at all concentrations. In contrast, titrations of Mnx WT with Cu showed increased binding to MnxF and MnxE with increasing Cu concentration (Figure 2D-F). Because high concentrations of Cu acetate caused significant peak broadening and reduced spectral quality, we only analyzed Cu addition up to 200  $\mu$ M. High concentration of added Mn did not lead to lower MS signal due to the turnover to insoluble  $\text{MnO}_2$ . Based on the metal-binding behavior of the released subunits, we speculate that the MnxE and MnxF may serve as reservoirs for the four essential Cu that bind to MnxG. Previous studies showed that 15 Cu ions are bound to the active Mnx complex from freshly prepared proteins.[18] Dialysis with Tris-buffer can reduce the number of bound Cu to 8, including 4 known catalytically relevant Cu in MnxG. The other 4 Cu have unknown functions, including 1 in MnxG and 3 in  $\text{MnxE}_3\text{F}_3$ .[19] Conformational changes during Mn(II) turnover may disrupt the bound Cu ions, as our proposed mechanism involves the traveling of  $\text{MnO}_2$  through the internal tunnel of MnxG and exiting from the central pore in the  $\text{MnxE}_3\text{F}_3$  hexamer ring.[9]

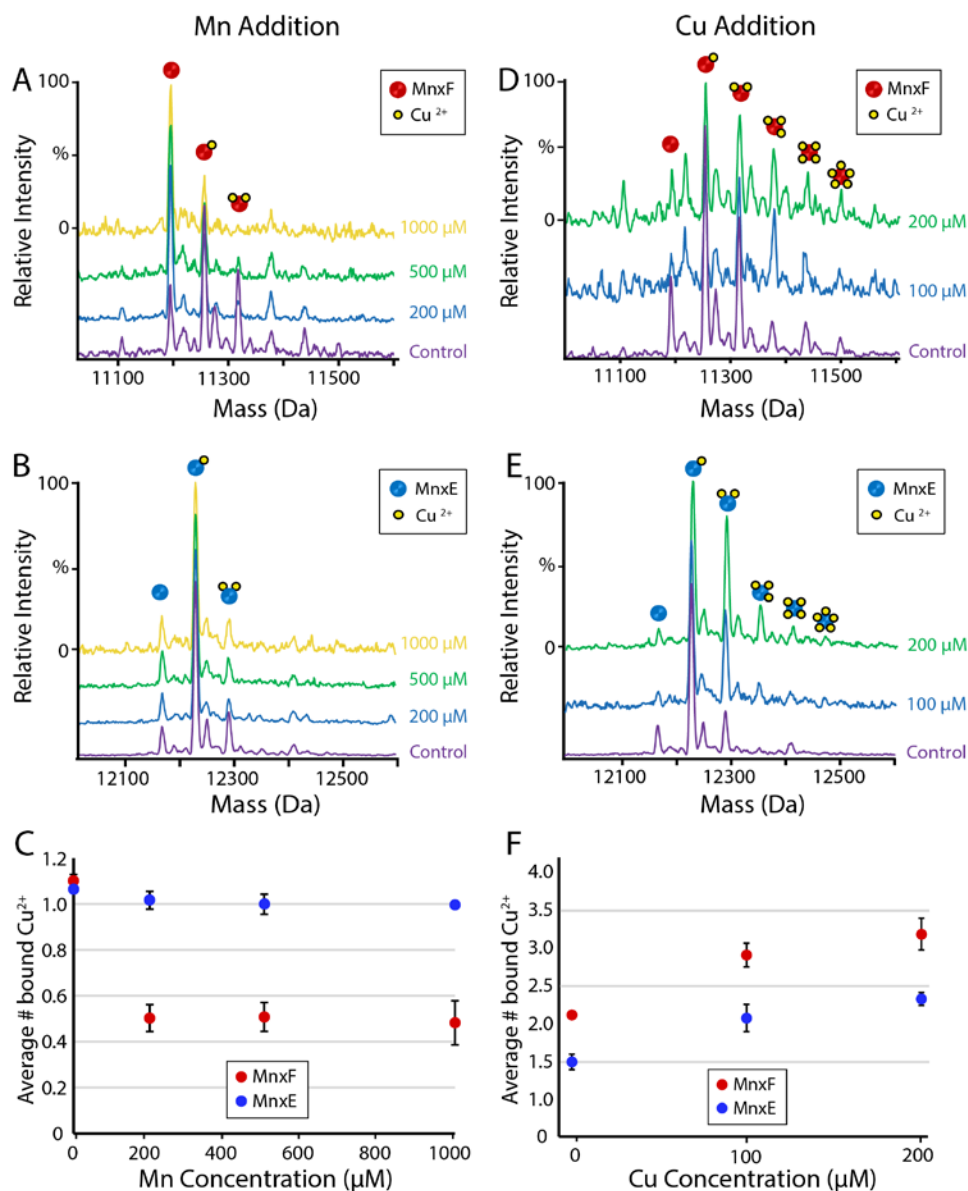


**Figure 2.** Effects of metal addition on MnxF and MnxE. The overlaid spectra of MnxF at 0 - 1000 μM Mn (A) show decreasing 2Cu and 1Cu peaks and an increasing apo peak as Mn concentration increases. Additional peaks beyond 2Cu visible in the controls are known artifacts reported previously. The overlaid spectra of MnxE under the same conditions show stability of the apo, 1Cu, and 2Cu peaks as Mn concentration increases (B). The average number of bound copper ions decreases significantly upon addition of Mn for MnxF, and the average number of bound Cu remains constant for MnxE (C). The overlaid spectra of MnxF at 0 - 200 μM Cu show increasing 2Cu, and 1Cu peaks and a decreasing apo peak as Cu concentration increases. 3Cu, 4Cu, and 5Cu peaks were also observed (D). The overlaid spectra of MnxE in response to Cu addition (E) also shows increasing Cu peaks and a decreasing apo peak as Cu concentration increases. The average number of bound copper ions increases for both MnxE and MnxF upon addition of Cu (F).

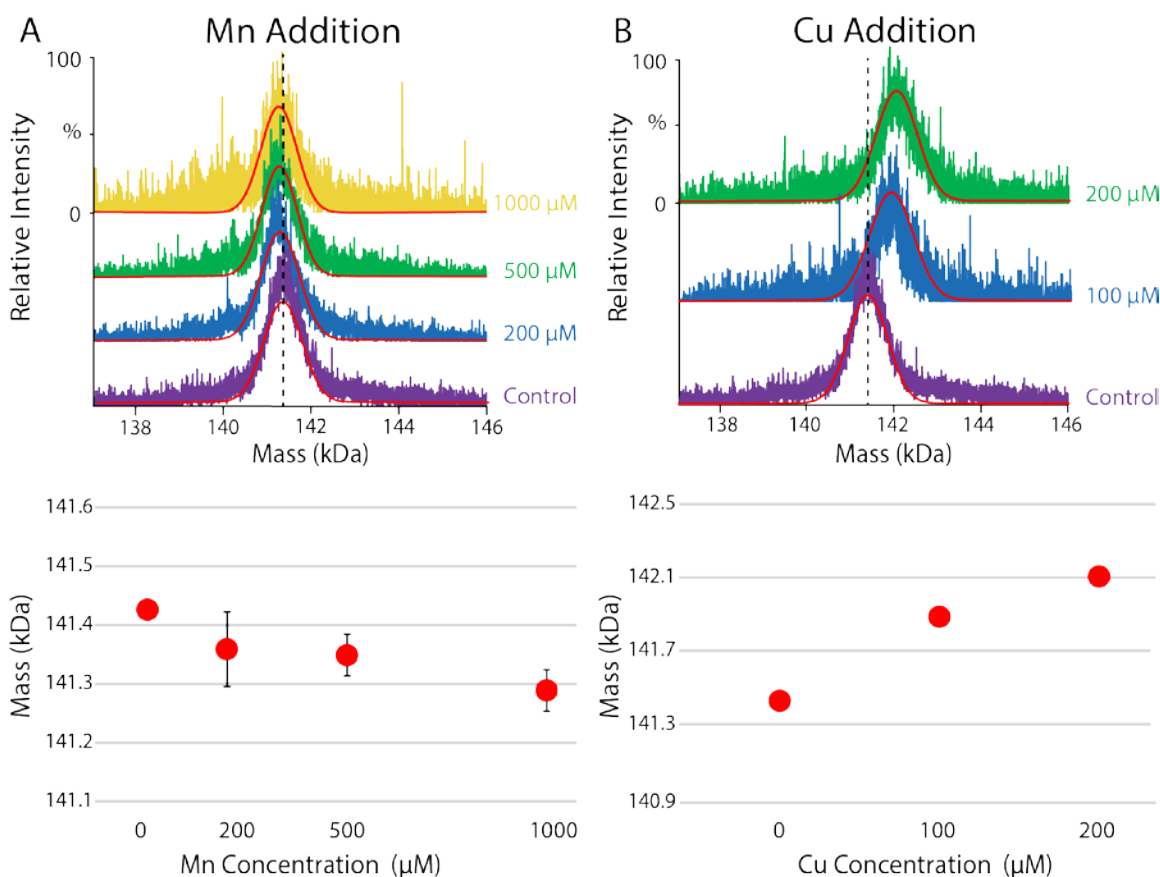


**Figure 3.** Metal addition results in a shift in mass for MnxG. A) Addition of Mn causes a slight shift toward lower mass, while addition of Cu (B) results in a more prominent shift toward higher mass. Gaussian fits (red peaks) are overlaid for each spectrum. A black dotted line marks the center of the control peak. The Gaussian peak maxima for each replicate were averaged to obtain the average mass for MnxG at each concentration of added metal, shown in a plot below each overlaid spectrum.

Mass resolving power was not sufficient to detect individual metal binding events for the larger MnxG subunit due to high heterogeneity.[12] Therefore, we used peak fitting to examine the average mass shifts of all MnxG populations in response to metal addition (Figure 3). Increasing concentrations of Mn resulted in a slight decrease in the mass of MnxG (Figure 3A) while Cu addition led to increased mass (Figure 3B). The decrease in mass indicates that the substrate turnover may involve some structural change that affects the binding of Cu in Mnx, possibly in a coordinated manner with MnxF which also showed significant loss of Cu. Indeed, previous circular dichroism spectroscopy measurements of the Mnx complex before and after addition of Mn(II) indicated enzyme conformational change,[10] which supported the mechanistically inferred activation mechanism of Mn(II) oxidation by Mnx. The increased binding of Cu to all Mnx subunits is also consistent with previous observation that extra Cu may fill additional sites

in the electron-transfer pathways necessary for Mn(II) turnover, thus making the cofactor inhibitory at high concentrations.[20]

#### *Ion mobility suggests conformational changes in Mnx during enzyme activity*

Sample data acquired in ion mobility mode also yield information regarding the shape of the complex, and, when coupled with SID, the shape of the dissociated monomeric species. This can be especially useful when evaluating changes in protein structure with changes in ligand binding, as well as other changes in sample conditions. Information on structural changes can be evaluated based on changes in drift time, with both shape and charge state affecting the measured drift time of a protein.[21] Thus, we extracted the drift time data for MnxE/F/G subunits and compared drift times with changes in Mn concentrations.

As expected, higher charge states of the same protein subunit had shorter drift times than lower charge states. Therefore, we separately compared drift times of different charge states. Similar to the mass analysis, we examined the drift times of apo and Cu binding species for MnxE and MnxF due to difficulty in directly capturing the Mn(II) states. For MnxG, we extracted the average drift times. Without Mn, MnxF exhibits shorter drift times than when it reacted with Mn. Subsequent titration of Mn beyond the initial addition did not lead to further changes in drift times (Figure 4). As shown in Figure 2, the decrease of Cu that occurs upon Mn addition also plateaus after the initial addition of Mn. This loss of Cu and the simultaneous shift to longer drift times suggests that MnxF may undergo a conformational change upon Mn addition, and the “activated state” has a reasonably well-defined conformation as shown by the consistently increased drift time. Interestingly, MnxE also exhibits a statistically significant change in drift time upon addition of Mn (Figure 4A) for the 3+ and 4+ charge states, despite retaining its bound copper throughout successive additions of Mn (Figure 2B). The pattern was consistent across all major charge states of MnxE and MnxF, except for MnxE 5+ which showed insignificant changes (Figure S1).

We also extracted drift time data for MnxE/F/G subunits upon Cu titration. ANOVA and Tukey's Honest Significant Difference post-hoc tests were used to determine if drift times were significantly different from one another at a 95% confidence level. Compared to Mn addition, fewer significant differences in drift time were detected for MnxE and MnxF, although they were not completely absent (Figure S2). Unfortunately, because the high concentrations of Cu acetate caused reduced spectral quality, low signal-to-noise at high Cu concentration resulted in more variability in the measurement, especially for the lower intensity 3+ and 5+ charge states. Besides improvement in signal, higher resolution IM and larger datasets than what is available in this study may help to elucidate the potential subtle structural changes that may occur in response to Cu binding. Nonetheless, we suspect these metal-induced conformational changes are functionally relevant, and may originate at least partially from the N-terminal regions of MnxE and MnxF. These regions were not resolved in the high resolution structure, and are likely dynamic.[9]

For MnxG, we evaluated the average drift time change in response to different metal concentrations without resolving individual binding events. Similar to MnxE and MnxF, MnxG showed a slight increase of drift time with Mn addition (Figure 5A), despite the slightly reduced mass (Figure 3A). The drift times were also similar for Mn addition above 200  $\mu\text{M}$ , possibly also corresponding to an activated state. In contrast, the drift time increase of MnxG exhibited more prominence upon Cu addition (Figure 5B), with gradual increases beyond 200  $\mu\text{M}$ . Given that significant mass increase after Cu addition was also observed for MnxG, the protein may be swelling from the extra bound metal ions. Overall, our results here echo the conformational change of the Mnx complex in response to Mn that has been observed by circular dichroism,[10] and additionally suggest structural changes of protein complexes may be retained in subunits released by SID.

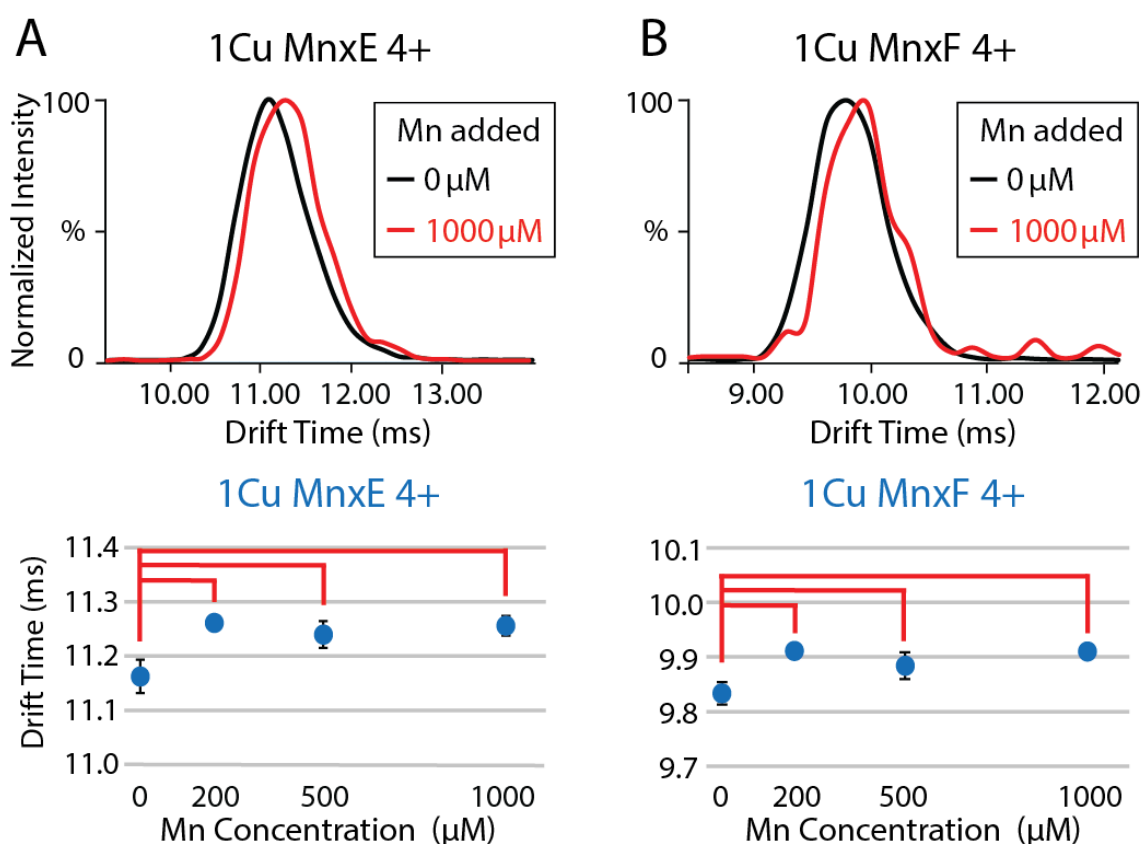
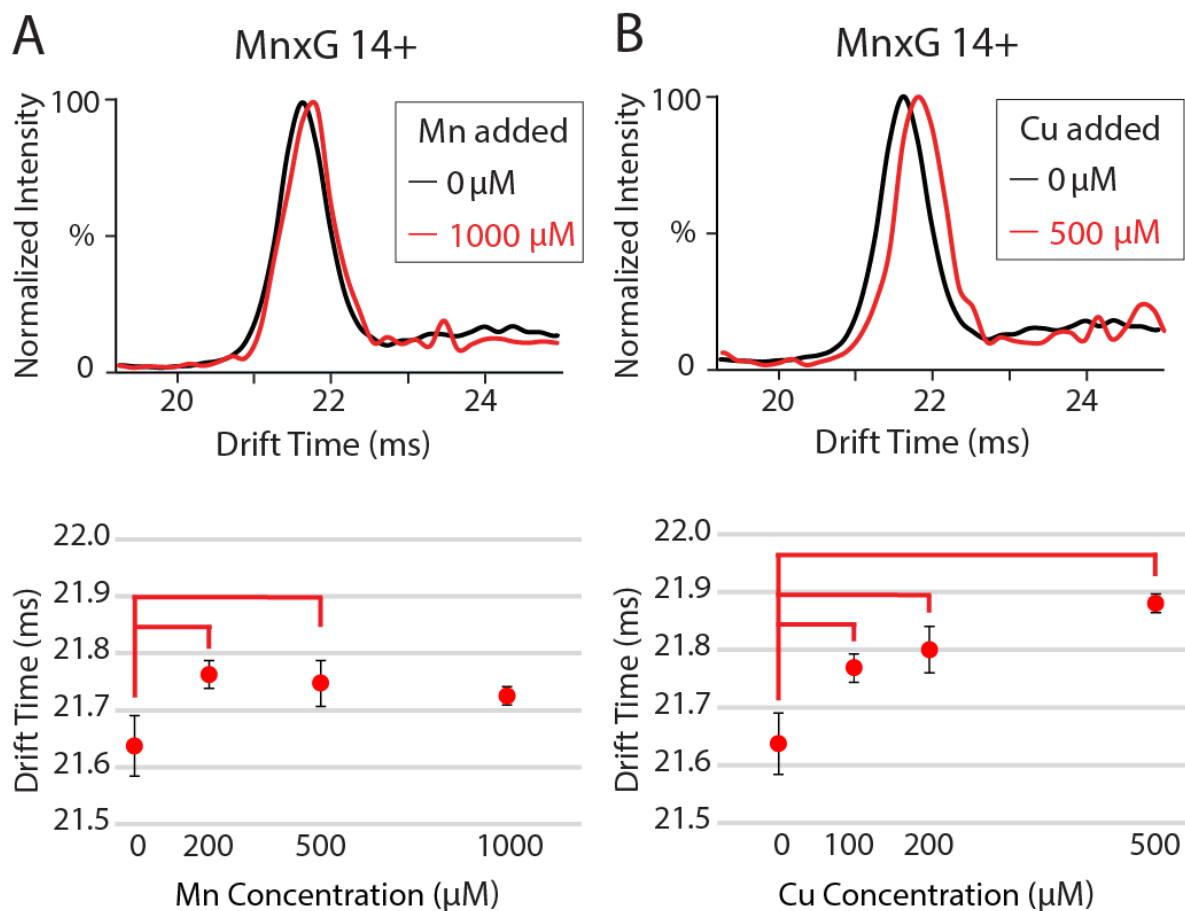


Figure 4. Changes in drift times of the 4+ charges state 1Cu peak of MnxE (A) and MnxF (B) subunits in response to Mn binding. The mobiligrams at the top of columns A and B show representative 1Cu-bound peaks of MnxE and MnxF at 0  $\mu\text{M}$  and 1000  $\mu\text{M}$  Mn. Average drift times at each concentration of Mn are plotted below each mobiligram. Red lines connecting two points indicate that the values are statistically different from one another ( $p < 0.05$ ).



**Figure 5.** Changes in average drift times for MnxDG upon metal binding. A) The drift time of MnxDG increases slightly upon addition of Mn despite downward shift in mass. B) MnxDG displays a prominent shift toward longer drift times upon addition of Cu. Because higher concentrations of Cu acetate caused significantly reduced spectral quality, we did not include Cu addition beyond 500 μM. Red lines connecting two points indicate that the values are statistically different from one another ( $p < 0.05$ ).

#### *Capturing Mn binding state with an inactive mutant H340A*

To better capture the Mn binding, we also investigated the interaction of Mn(II) substrate with an inactive mutant, MnxDG H340A,[9, 14] where histidine 340 was mutated to alanine in the MnxDG sequence. Even with the use of this inactive mutant, binding of Mn on MnxDG monomers was difficult to detect. For this reason, experiments conducted at 20 mM AA concentration were completed. The use of lower AA concentrations to study protein-metal binding by native MS has been completed by others previously[22, 23] and has been shown to affect complexes that are sensitive to ionic strength.[24] In addition acetate may compete with protein for metal binding, making weak protein-metal interactions difficult to detect.[25] A moderate shift to increased Mn binding to MnxDG H340A subunits was observed at this reduced AA concentration (Figure 6). Several Mn adducts bound to MnxDG and MnxDG were found, including Mn bound to Cu-bound

species, suggesting Mn binding does not prevent Cu binding and likely occupies a different site, similar to the catalytic MnxG where previous metal-inhibition studies indicated Cu did not compete with Mn.[20] Overnight Mnx H340A incubations with Mn(II) substrate revealed a clear direct correlation between Mn(II) solution concentration and the amount of Mn adducts for MnxF and MnxE subunits. Although the detailed binding state cannot be resolved, the MnxG subunit depicted peak broadening and shifting to higher mass most likely due to binding with Mn(II) (Figure 7A). Reducing AA concentration in the experiments with Mnx WT to probe Mn-substrate binding still did not lead to detection of well resolved Mn-bound species. Instead, oxidation of all protein subunits was observed, particularly for MnxE (Figure 7B). This was not unexpected given the formation of MnO<sub>2</sub> in WT, which serves as catalyst for oxidation. Further analysis is required to determine the biological significance of this oxidation behavior. These results highlight the importance of optimizing solution conditions and the value of probing changes in metal binding by native MS between active and inactive enzyme states to parse subunit function, particularly for weak or transient interactions that may otherwise go undetected under a particular native MS solution condition.

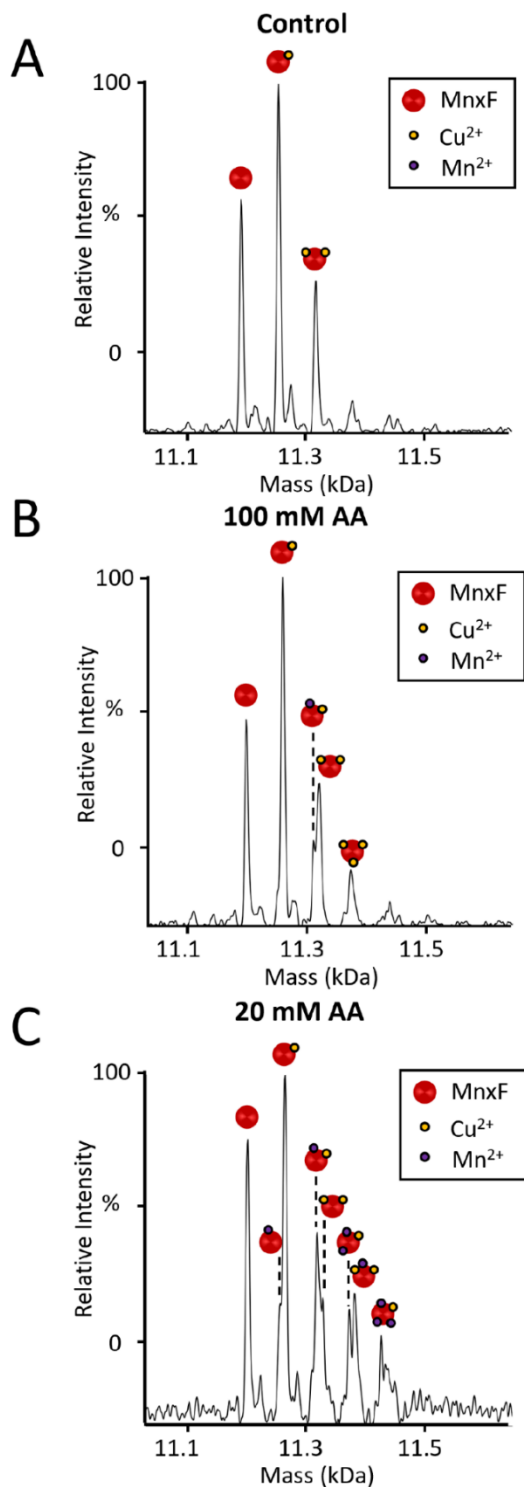


**Figure 6.** Analysis of Mn binding to MnxF subunits after subunit dissociation. MnxF H340A Mn<sup>4+</sup> charge state after 100 V SID with A) 0  $\mu$ M Mn control sample compared with 500  $\mu$ M Mn samples in either B) 100 mM or C) 20 mM AA, with Cu and Mn bound peaks labeled in each spectrum.

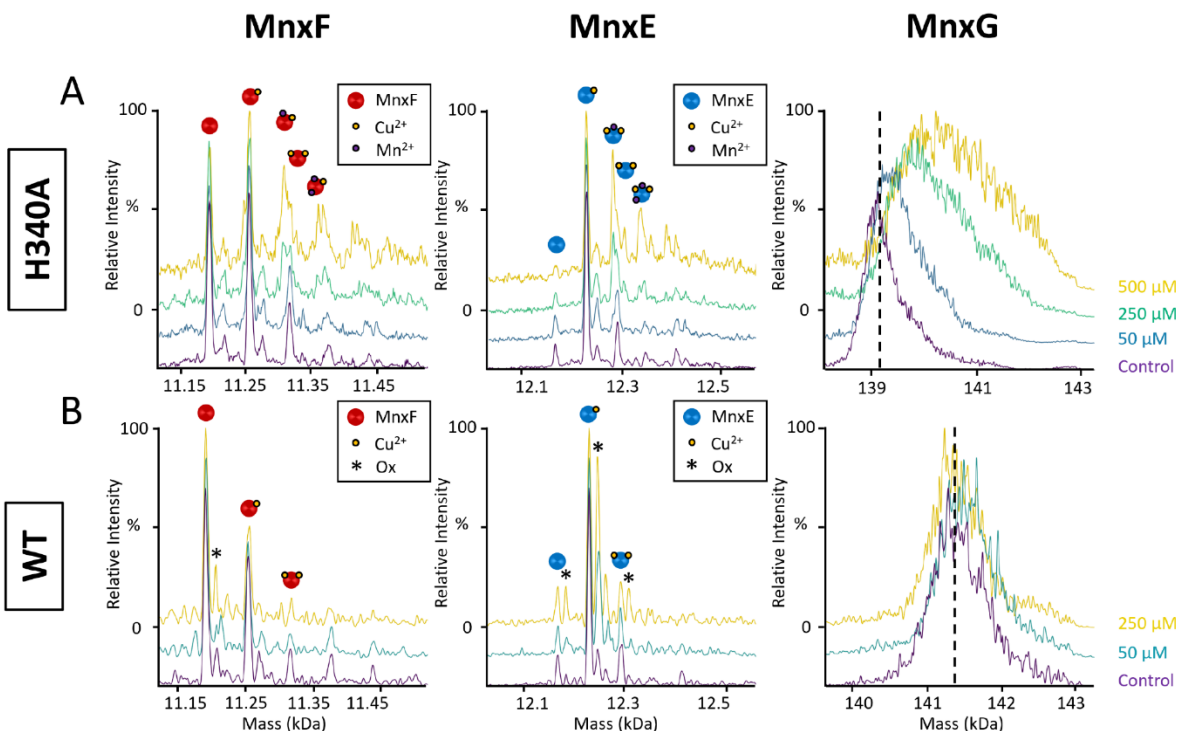


**Figure 7.** Degree of Mn binding after overnight incubation with A) 0 – 500  $\mu\text{M}$  Mn for H340A and B) 0 – 250  $\mu\text{M}$  Mn for WT Mnx sample MnxE/F/G monomers when samples were prepared in 20 mM AA. Oxidation (Ox) of MnxF and MnxE was observed with WT samples.

## Conclusions

We have shown that SID coupled with ion mobility and native MS is a useful tool for obtaining unique metal binding information of a multicopper oxidase complex Mnx. By using SID, we can release subunits from intact protein complexes and separately investigate the contribution of individual subunits. With our current instrument resolving power, we can ascertain the identity and number of bound metal ligands on MnxE and MnxF, while monitoring the average change of all MnxG populations without resolving individual binding stoichiometry. Analysis via ion mobility provides additional information on protein shape and subunit-specific information that standard enzymatic assays are unable to obtain. The changes of bound Cu and drift time in response to substrate turnover suggest structural change of the protein during its activity, which is consistent with orthogonal measurement by circular dichroism.[10] Future experiments with higher mass and ion mobility resolving power[26-30] may reveal more subtle changes. Introducing native top-down methods could also add more detailed information such as metal binding sites to decipher the mechanism.[7, 22, 31, 32] In addition to new advances in MS technology, our data also show how sample preparation such as buffer composition can impact measured metal binding. The continued development of these MS technologies would yield powerful new avenues for investigating other multisubunit and heterogenous enzyme systems.

## **Acknowledgements**

The work was performed at the Environmental Molecular Science Laboratory (EMSL), a Department of Energy (DOE) Office of Science User Facility sponsored by the Office of Biological and Environmental Research, under project 50773 (<https://doi.org/10.46936/lser.proj.2019.50773/60000097>). We thank Prof. Vicki Wysocki's group at the Ohio State University for helping with instrument modification (supported by NIH National Institute of General Sciences P41GM128577). We also acknowledge the National Science Foundation: award numbers CHE-1807222 and EAR-1951143 to TGS; and CHE-1807158, CHE-2120408 and EAR-2122086 to BMT.

## **Data statement**

All mass spectrometry raw data files that support the findings of this study are openly available at <https://massive.ucsd.edu/ProteoSAFe/dataset.jsp?task=0b6b5385e4c84e638d5a2df5c77d8958>. (User: MSV000092552. Password: Prm5018).

## Supplemental Figures

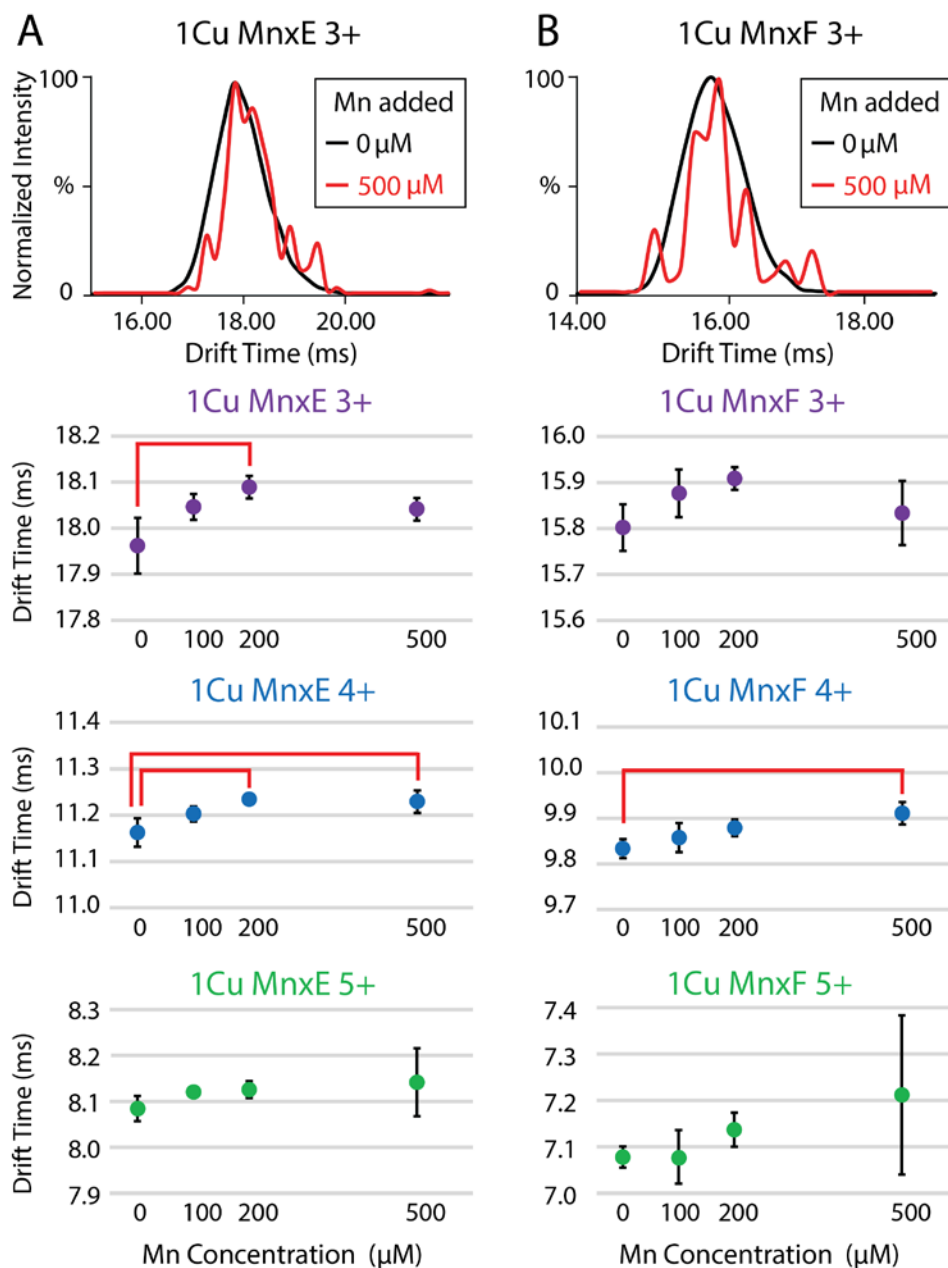


**Figure S1.** Drift time changes of the 3+, 4+, and 5+ charge state 1Cu peak of MnxE (A) and MnxF (B) subunits in response to addition of copper. The mobiligrams at the top of columns A and B show representative 3+ charge state 1Cu-bound peaks at 0  $\mu\text{M}$  and 500  $\mu\text{M}$  Cu. Average drift times at each concentration of Cu are plotted below each mobiligram. Red lines connecting two points indicate that the values are statistically different from one another ( $p < 0.05$ ).

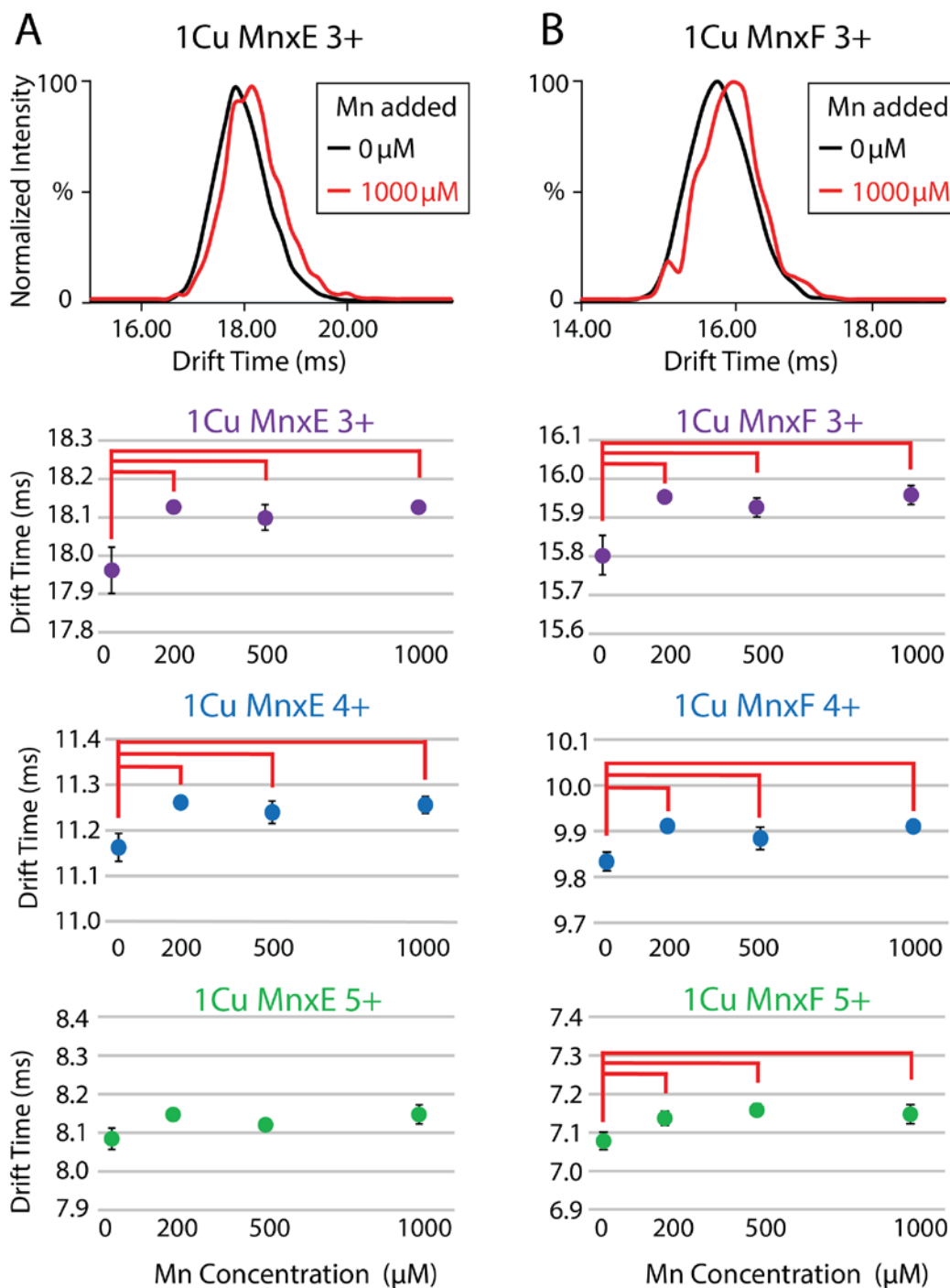


**Figure S2.** Drift time changes of the 3+, 4+, and 5+ charge state 1Cu peak of MnxE (A) and MnxF (B) subunits in response to addition of manganese. The mobiligrams at the top of columns A and B show representative 3+ charge state 1Cu-bound peaks at 0  $\mu\text{M}$  and 1000  $\mu\text{M}$  Mn. Average drift times at each concentration of Mn are plotted below each mobiligram. Red lines connecting two points indicate that the values are statistically different from one another ( $p < 0.05$ ).

## References

- [1] V. Lažetić, E.R. Troemel, Conservation lost: host-pathogen battles drive diversification and expansion of gene families, *The FEBS Journal*, 288 (2021) 5289-5299.
- [2] S. Gad, S. Ayakar, Protein scaffolds: A tool for multi-enzyme assembly, *Biotechnology Reports*, 32 (2021) e00670.
- [3] X. Lv, S. Cui, Y. Gu, J. Li, G. Du, L. Liu, Enzyme Assembly for Compartmentalized Metabolic Flux Control, *Metabolites*, 10 (2020) 125.
- [4] M.D. Miller, G.N. Phillips, Moving beyond static snapshots: Protein dynamics and the Protein Data Bank, *Journal of Biological Chemistry*, 296 (2021) 100749.
- [5] E. Boeri Erba, L. Signor, C. Petosa, Exploring the structure and dynamics of macromolecular complexes by native mass spectrometry, *Journal of Proteomics*, 222 (2020) 103799.
- [6] E.G. Marklund, J.L. Benesch, Weighing-up protein dynamics: the combination of native mass spectrometry and molecular dynamics simulations, *Curr Opin Struct Biol*, 54 (2019) 50-58.
- [7] M. Zhou, C. Lantz, K.A. Brown, Y. Ge, L. Paša-Tolić, J.A. Loo, F. Lermyte, Higher-order structural characterisation of native proteins and complexes by top-down mass spectrometry, *Chemical Science*, 11 (2020) 12918-12936.
- [8] C.A. Romano, M. Zhou, Y. Song, V.H. Wysocki, A.C. Dohnalkova, L. Kovarik, L. Paša-Tolić, B.M. Tebo, Biogenic manganese oxide nanoparticle formation by a multimeric multicopper oxidase Mnx, *Nature Communications*, 8 (2017) 746-746.
- [9] I.V. Novikova, A.V. Soldatova, S. Thibert, C. Romano, M. Zhou, B.M. Tebo, J.E. Evans, T.G. Spiro, Cryo-EM Structure of the Mnx Protein Complex Reveals a Tunnel Framework for the Mechanism of Manganese Biomineralization, under review.
- [10] A.V. Soldatova, L. Tao, C.A. Romano, T.A. Stich, W.H. Casey, R.D. Britt, B.M. Tebo, T.G. Spiro, Mn(II) Oxidation by the Multicopper Oxidase Complex Mnx: A Binuclear Activation Mechanism, *Journal of the American Chemical Society*, 139 (2017) 11369-11380.
- [11] A.V. Soldatova, C.A. Romano, L. Tao, T.A. Stich, W.H. Casey, R.D. Britt, B.M. Tebo, T.G. Spiro, Mn(II) Oxidation by the Multicopper Oxidase Complex Mnx: A Coordinated Two-Stage Mn(II)/(III) and Mn(III)/(IV) Mechanism, *Journal of the American Chemical Society*, 139 (2017) 11381-11391.
- [12] M. Zhou, J. Yan, C.A. Romano, B.M. Tebo, V.H. Wysocki, L. Paša-Tolić, Surface Induced Dissociation Coupled with High Resolution Mass Spectrometry Unveils Heterogeneity of a 211 kDa Multicopper Oxidase Protein Complex, *Journal of the American Society for Mass Spectrometry*, 29 (2018) 723-733.
- [13] C.N. Butterfield, A.V. Soldatova, S.-W. Lee, T.G. Spiro, B.M. Tebo, Mn(II,III) oxidation and MnO<sub>2</sub> mineralization by an expressed bacterial multicopper oxidase, *Proceedings of the National Academy of Sciences*, 110 (2013) 11731-11735.
- [14] L. Tao, T.A. Stich, C.N. Butterfield, C.A. Romano, T.G. Spiro, B.M. Tebo, W.H. Casey, R.D. Britt, Mn(II) Binding and Subsequent Oxidation by the Multicopper Oxidase MnxG Investigated by Electron Paramagnetic Resonance Spectroscopy, *Journal of the American Chemical Society*, 137 (2015) 10563-10575.
- [15] D.T. Snyder, E.M. Panczyk, A. Somogyi, D.A. Kaplan, V. Wysocki, Simple and minimally invasive SID devices for native mass spectrometry, *Analytical Chemistry*, 92 (2020) 11195-11203.
- [16] D.J. Reid, J.M. Diesing, M.A. Miller, S.M. Perry, J.A. Wales, W.R. Montfort, M.T. Marty, MetaUniDec: High-Throughput Deconvolution of Native Mass Spectra, *Journal of the American Society for Mass Spectrometry*, 30 (2019) 118-127.
- [17] S.E. Haynes, D.A. Polasky, S.M. Dixit, J.D. Majmudar, K. Neeson, B.T. Ruotolo, B.R. Martin, Variable-Velocity Traveling-Wave Ion Mobility Separation Enhancing Peak Capacity for Data-Independent Acquisition Proteomics, *Analytical Chemistry*, 89 (2017) 5669-5672.
- [18] C.N. Butterfield, B.M. Tebo, Substrate specificity and copper loading of the manganese-oxidizing multicopper oxidase Mnx from *Bacillus* sp. PL-12, *Metallomics*, 9 (2017) 183-191.

- [19] L. Tao, T.A. Stich, S.H. Liou, A.V. Soldatova, D.A. Delgadillo, C.A. Romano, T.G. Spiro, D.B. Goodin, B.M. Tebo, W.H. Casey, R.D. Britt, Copper Binding Sites in the Manganese-Oxidizing Mnx Protein Complex Investigated by Electron Paramagnetic Resonance Spectroscopy, *Journal of the American Chemical Society*, 139 (2017) 8868-8877.
- [20] A.V. Soldatova, W. Fu, C.A. Romano, L. Tao, W.H. Casey, R.D. Britt, B.M. Tebo, T.G. Spiro, Metallo-inhibition of Mnx, a bacterial manganese multicopper oxidase complex, *Journal of Inorganic Biochemistry*, 224 (2021) 111547.
- [21] G. Ben-Nissan, M. Sharon, The application of ion-mobility mass spectrometry for structure/function investigation of protein complexes, *Current Opinion in Chemical Biology*, 42 (2018) 25-33.
- [22] P. Wongkongkathep, J.Y. Han, T.S. Choi, S. Yin, H.I. Kim, J.A. Loo, Native Top-Down Mass Spectrometry and Ion Mobility MS for Characterizing the Cobalt and Manganese Metal Binding of  $\alpha$ -Synuclein Protein, *Journal of the American Society for Mass Spectrometry*, 29 (2018) 1870-1880.
- [23] E.M. Martin, F.D.L. Kondrat, A.J. Stewart, J.H. Scrivens, P.J. Sadler, C.A. Blindauer, Native electrospray mass spectrometry approaches to probe the interaction between zinc and an anti-angiogenic peptide from histidine-rich glycoprotein, *Scientific Reports*, 8 (2018) 8646.
- [24] A.F.M. Gavriilidou, B. Gülbakan, R. Zenobi, Influence of Ammonium Acetate Concentration on Receptor–Ligand Binding Affinities Measured by Native Nano ESI-MS: A Systematic Study, *Analytical Chemistry*, 87 (2015) 10378-10384.
- [25] T.R. Young, Z. Xiao, Principles and practice of determining metal–protein affinities, *Biochemical Journal*, 478 (2021) 1085-1116.
- [26] A.R. Todd, L.F. Barnes, K. Young, A. Zlotnick, M.F. Jarrold, Higher Resolution Charge Detection Mass Spectrometry, *Analytical Chemistry*, 92 (2020) 11357-11364.
- [27] J.N. Dodds, E.S. Baker, Ion Mobility Spectrometry: Fundamental Concepts, Instrumentation, Applications, and the Road Ahead, *Journal of the American Society for Mass Spectrometry*, 30 (2019) 2185-2195.
- [28] K. Giles, J. Ujma, J. Wildgoose, S. Pringle, K. Richardson, D. Langridge, M. Green, A Cyclic Ion Mobility-Mass Spectrometry System, *Analytical Chemistry*, 0 (2019) null-null.
- [29] Y.M. Ibrahim, A.M. Hamid, L. Deng, S.V.B. Garimella, I.K. Webb, E.S. Baker, R.D. Smith, New frontiers for mass spectrometry based upon structures for lossless ion manipulations, *Analyst*, 142 (2017) 1010-1021.
- [30] F.C. Liu, M.E. Ridgeway, M.A. Park, C. Bleiholder, Tandem-trapped ion mobility spectrometry/mass spectrometry (tTIMS/MS): a promising analytical method for investigating heterogenous samples, *Analyst*, (2022).
- [31] F. Lermyte, J. Everett, Y.P.Y. Lam, C.A. Wootton, J. Brooks, M.P. Barrow, N.D. Telling, P.J. Sadler, P.B. O'Connor, J.F. Collingwood, Metal Ion Binding to the Amyloid beta Monomer Studied by Native Top-Down FTICR Mass Spectrometry, *Journal of the American Society for Mass Spectrometry*, 30 (2019) 2123-2134.
- [32] C.M. Crittenden, E.T. Novelli, M.R. Mehaffey, G.N. Xu, D.H. Giles, W.A. Fies, K.N. Dalby, L.J. Webb, J.S. Brodbelt, Structural Evaluation of Protein/Metal Complexes via Native Electrospray Ultraviolet Photodissociation Mass Spectrometry, *Journal of the American Society for Mass Spectrometry*, 31 (2020) 1140-1150.